



Full Text View

[Volume 31, Issue 12 \(December 2001\)](#)

Journal of Physical Oceanography

Article: pp. 3551–3568 | [Abstract](#) | [PDF \(234K\)](#)

The Cross-Stream Potential Vorticity Front and Its Role in Meander-Induced Exchange in the Gulf Stream

J. Rajamony

Atmospheric and Environmental Research, Inc., Lexington, Massachusetts

D. Hebert and T. Rossby

Graduate School of Oceanography, University of Rhode Island, Narragansett, Rhode Island

(Manuscript received April 11, 2000, in final form May 25, 2001)

DOI: 10.1175/1520-0485(2001)031<3551:TCSPVF>2.0.CO;2

ABSTRACT

The potential vorticity (PV) front observed in the upper thermocline at the northern edge of the Gulf Stream has been thought of as an inhibitor to lateral motion of parcels on isopycnals. The role of the PV front in relation to lateral motion and cross-stream exchange was investigated by monitoring the evolving PV field in the vicinity of Lagrangian parcels at the northern edge of the stream. The observational study involved shipboard acoustic Doppler current profiler (ADCP) and conductivity–temperature–depth surveys to sample the velocity and density fields around water parcels as they flowed through meanders. The observations reveal that the PV field in the vicinity of parcels moves laterally across the stream and evolves as parcels negotiate meander crests and troughs, allowing parcels to move across the stream without changing their Lagrangian PV. This lateral motion of the PV front suggests that it is more a response to than an inhibitor of the lateral motion of parcels in the meanders. The relative contributions of the components of PV to the front indicated a rich structure of changes in shear and stretching across the stream. Also, temperature changes of Lagrangian parcels were linked to small-scale mixing processes associated with observed intrusive features. Estimated diffusion coefficients suggest that horizontal mixing could be the main mechanism of mixing in the upper thermocline at the northern edge of the stream.

Table of Contents:

- [Introduction](#)
- [Data and methods](#)
- [Results](#)
- [Discussion](#)
- [Summary](#)
- [REFERENCES](#)
- [APPENDIX](#)
- [TABLES](#)
- [FIGURES](#)

Options:

- [Create Reference](#)
- [Email this Article](#)
- [Add to MyArchive](#)
- [Search AMS Glossary](#)

Search CrossRef for:

- [Articles Citing This Article](#)

Search Google Scholar for:

- [J. Rajamony](#)
- [D. Hebert](#)
- [T. Rossby](#)

1. Introduction

Midlatitude jets that separate subtropical and subtropical gyres play an important role in the exchange of properties between the gyres. The exchange is an important term in gyre-wide balance of properties such as heat, momentum, and potential vorticity (Yang 1996a,b; Holland and Rhines 1980; Lozier and Riser 1989). This meridional intergyre exchange is also important from the perspective of climate variability. In the North Atlantic, where the Gulf Stream and the North Atlantic Current separate the gyres, the subpolar gyre is the formation region of intermediate and deep water masses that go into the thermohaline circulation (Schmitz and McCartney 1993); the intergyre transport across the jet is therefore of special importance. To model the role of the Gulf Stream in the global climate system, it is necessary to understand the process of exchange across the stream and the mixing of stream water into the recirculation gyres.

There are various means by which intergyre transport can be effected across a midlatitude jet. Formation of rings by steep meanders and the interaction of previously formed rings with the stream are two mechanisms that lead to intergyre transport (Lai and Richardson 1977; Lillibridge and Hummon 1990; Song et al. 1995). The lateral motion of water parcels in the meanders of the Gulf Stream may also result in exchange between the gyres (Bower and Rossby 1989; Bower 1991; Song et al. 1995); this third mechanism will be referred to as meander-induced exchange. Bower et al. (1985) and Bower and Rossby (1989) concluded that ring shedding was not a principal pathway of exchange between the gyres in the main thermocline, but that mixing must occur on scales smaller than $O(30 \text{ km})$. Consistent with that conclusion, the float study by Song et al. (1995) suggested that the meander-induced mechanism of exchange is the largest of the three mechanisms.

Water parcels in Gulf Stream meanders were observed to move laterally onshore(offshore) and upwell(downwell) as they approach meander crests(troughs) (Owens 1984; Bower and Rossby 1989; Song et al. 1995) and when these meander-induced lateral motions attain large amplitudes, water parcels may be exchanged between the stream and surroundings. Larger meander-induced lateral motions on deep isopycnals compared to shallow ones has been a striking feature in the observations of meander-induced lateral motions (e.g., Song et al. 1995). Since the observation of cross-stream migration of parcels in the stream more than a decade ago, two hypotheses concerning meander-induced exchange and its depth dependence have been advanced. The first argument is that the cross-stream potential vorticity (PV) gradient, usually observed on the cyclonic side of the stream due to the large velocity shear and layer-thickness change, acts as a fixed “barrier” to inhibit lateral motions in the stream (Bower et al. 1985; Lozier and Riser 1989). Since the PV contrast between the two sides of the stream diminishes with depth (Bower and Lozier 1994), this argument is consistent with the observed depth dependence of meander-induced exchange. The second hypothesis is based on the kinematics of the stream and argues that enhanced cross-stream motion takes place below a steering level where the downstream velocity of the parcel equals the phase speed of the propagating meander (Owens 1984; Bower 1991; Lozier et al. 1997). Above the steering level, the meander is essentially a stationary wave for the particle to flow through, while below the steering level the particle is left behind by the propagating meander. In this hypothesis, water parcels are not dynamically constrained to conserve potential vorticity. This manuscript deals with the first hypothesis.

The exchange between Gulf Stream and surroundings has been studied before from the point of view of potential vorticity (Bower 1989; Song and Rossby 1997). A study of how the components of PV adjust among one another tells us about evolution of density and velocity fields. Changes in Lagrangian PV would be indicative of dissipative or generative processes. Studies of PV in the stream by using isopycnal Lagrangian floats by Bower (1989) in the lower thermocline and by Song and Rossby (1997) in the upper thermocline assumed PV conservation and considered PV as consisting of four components—planetary, cross-frontal shear, curvature, and stretching. Thus PV may be expressed as

$$PV = \left(f + \frac{\partial v}{\partial n} + \kappa v \right) / H, \quad (1)$$

where f is planetary vorticity, v is along-trajectory velocity, n is the cross-trajectory axis, κ is the curvature of the float trajectory, and H is the thickness of the water parcel tracked by the float (see appendix A for details). It is the robustness of the cross-stream structure of the velocity field that makes the division of relative vorticity into shear and curvature components useful: a given change in the cross-stream position of a parcel, irrespective of its downstream position, would correspond to the same change in its shear vorticity. Since the frozen-field nature of the cross-stream velocity field is disturbed more in the upper than in the lower thermocline at meander extrema by inertial effects, such a division may not be as useful in the upper thermocline as it is in the lower thermocline.

Of the four components of PV, these float studies could measure only planetary and curvature vorticities. Shear vorticity was estimated based on a frozen velocity field [Halkin and Rossby (1985) or its modified version, which accounts for inertial effects at meander extrema, Hummon (1995)], and stretching vorticity was estimated as a residual under the assumption of PV conservation. Bower's (1989) main conclusions include (i) parcels move onshore(offshore) and upwell(downwell) along isopycnals, on approaching a crest(trough); (ii) the principal PV balance is among shear, stretching, and curvature vorticities, with curvature vorticity playing a less important role on the cyclonic side of the stream; and (iii) on the anticyclonic side of the stream horizontal divergence(convergence) occurs downstream of meander troughs(crests), while the pattern is reversed on the cyclonic side. Song and Rossby's (1997) results are in general agreement with the above; the

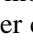
pattern of divergence and convergence were found to be opposite to each other in the case of growing and decaying meanders; Bower's results apply for the growing meander case.

In this study, the evolving velocity and density fields at and around Lagrangian parcels were measured by shipboard surveys; thus all four components of PV were measured. Previously only water parcels in the stream were studied; here water parcels entering and leaving the stream were also studied. Unlike previous studies, PV conservation was not assumed here, but could be tested since all PV components were measured. PV cross sections of the stream, on either side of a parcel, were constructed on the isopycnal of the parcel at various downstream locations. From these sections, the evolution of the parcel's PV and the PV structure in which the parcel was embedded were studied. While the measured PV of the tracked parcel can be thought of as Lagrangian PV, the PV sections are not Lagrangian sections since the parcels neighboring the tracked parcel will be different at different cross sections due to the large horizontal velocity shear in the stream. The objective of this paper is to study the evolution of PV around Lagrangian parcels and to understand the cross-stream motion of Lagrangian parcels in the context of the cross-stream PV front. The onshore side (i.e., the cyclonic side) of the upper thermocline (15°C) in the stream was chosen for this Lagrangian study, since it is here that the PV front has been observed to be most prominent (Bower and Lozier 1994). In addition, mixing of temperature and PV were also studied based on the extensive survey of these properties around parcels in the stream.

A description of the field study, the data collected, and their analysis are presented in the next section. The observations of PV fronts, Lagrangian PV, and their evolution are described in [section 3](#). The implication of these results, the need to reexamine the hypothesis that the PV front acts as a barrier, and a discussion of mixing and exchange at the northern edge of the Gulf Stream are presented in [section 4](#).


2. Data and methods

a. Description of the parcels/floats, CTD, and ADCP surveys

To study the evolution of Lagrangian PV and the role of the PV front in exchange processes, water parcels on the isopycnal $\sigma_\theta = 26.6$, in the upper thermocline, were tracked at the northern edge of the Gulf Stream during two cruises. A detailed description of the sampling procedure and the data collected during the two cruises is given in [Rajamony et al. \(1997\)](#). As a parcel moved downstream, the ship moved with it and sampled the evolving density and velocity fields in its vicinity with shipboard CTD and acoustic Doppler current profiler (ADCP) surveys ([Fig. 1](#) ). During the first cruise (in late spring of 1995) PV fields around three parcels were studied—one negotiating a meander trough, one upstream of a crest, and one downstream of a crest. The trajectories of these parcels (referred to as P1, P2, and P3 for the rest of this manuscript) were computed numerically by using CTD and ADCP data as described in [Rajamony et al. \(1999\)](#). The CTD and ADCP data were used to create velocity maps on isopycnals and trajectories of the isopycnal parcels were determined by integrating these velocities with respect to time. During the second cruise (in early fall 1995) PV fields around two parcels were studied—both upstream of a meander crest. The trajectories of these parcels (referred to as F1 and F2, for the rest of this manuscript), tagged with acoustically tracked isopycnal Swallow floats, were also computed numerically by using density and velocity data from CTD and ADCP surveys. The tracks of F1 and F2 determined with the CTD and ADCP data were used in this study for the sake of consistency with the earlier cruise. Over the course of a day, the parcel trajectory estimated with CTD and ADCP differed from the trajectory of an acoustically tracked isopycnal float by about 2 km ([Rajamony et al. 1999](#)), with this difference almost evenly spread between the along-trajectory and cross-trajectory directions.

The CTD and ADCP data collected in the vicinity of the parcels were used to construct cross sections of temperature and PV in the stream, in the neighborhood of the parcels at various downstream distances; while referring to these near-synoptic sections, the term “Eulerian” will be used. By using the known positions of the parcels in these cross sections, the Lagrangian temperature and PV of the parcels were also determined from the sections. These calculations are described in [section 2b](#).

b. Calculation of Eulerian PV sections across the stream following the parcel

While sampling the density and velocity fields on either side of a parcel trajectory, the ship crossed the stream in the neighborhood of the parcel out to distances of about 7 km on either side of the parcel. Most of these crossings were almost perpendicular to the stream, and data collected during these near-perpendicular crossings were used to construct PV cross sections of the stream around the parcel ([Fig. 2](#) ). The following six-step process was adopted to construct the PV sections.

1. For each crossing of the stream in the vicinity of the parcel, the velocity and density (from ADCP and CTD surveys, respectively) were interpolated onto a depth grid.
2. The direction and curvature of the parcel's trajectory at each of these crossings were determined from the known

trajectory of the tracked parcel. If x and y are the known coordinates of the parcel, then

the direction of the trajectory,

$$\theta = \tan^{-1}(y')$$

and the curvature of the trajectory,

$$\kappa = \frac{y''}{(1 + y'^2)^{3/2}},$$

where

$$y' = \frac{dy}{dx}, \text{ etc.}$$

3. The data line was projected on the direction perpendicular to the trajectory by using θ ; ρ and \mathbf{v} were interpolated to a regularly spaced grid of depth versus cross-trajectory distance, to obtain $\rho(x, z)$ and $\mathbf{v}(x, z)$, where x is now the cross-trajectory direction and y is along the trajectory. The origin for x was conveniently chosen corresponding to the depth of a given isopycnal (see later for details); thus changes in particle position, velocity structure, and PV structure were measured with respect to the density structure.
4. The density and velocity data were smoothed over a horizontal scale of 5 km, prior to calculating PV from density and velocity gradients. (Five-kilometer smoothed data were not used to determine the trajectory of the parcels as described in [section 2a](#); the only smoothing in that case was what is inherent in integration.) This scale was chosen based on previous observations that the lengthscale of the cross-stream PV front is greater than 10 km ([Bower and Lozier 1994](#)). Also, for horizontal eddy diffusivities determined with the unsmoothed data ([section 4](#)) of $O(10\text{--}100 \text{ m}^2 \text{ s}^{-1})$, 3–5 km is the horizontal scale below which properties will not be conserved over $O(2 \text{ days})$, which was the observed entrainment/detrainment timescale in the upper thermocline. From the smoothed data on the grid, $\partial\rho/\partial x$, $\partial\rho/\partial z$, $\partial\mathbf{v}/\partial x$, and $\partial\mathbf{v}/\partial z$ were calculated. (Here \mathbf{v} is the along-trajectory velocity and x is the cross-trajectory direction.) Potential vorticity was then determined as

$$\text{PV}(x, z) = -\frac{1}{\rho} \frac{\partial\rho}{\partial x} \frac{\partial v}{\partial z} + \frac{1}{\rho} \frac{\partial\rho}{\partial z} \left(f + \frac{\partial v}{\partial x} + \kappa v \right) \quad (2)$$

at each grid point. The relation between [Eqs. \(1\) and \(2\)](#) can be found in [Bower \(1989\)](#) or in [appendix A](#).

5. Potential vorticity was mapped onto density surfaces. That is, $\text{PV}(x, \rho)$ was determined by using $\rho(x, z)$ and $\text{PV}(x, z)$.
6. On the parcel's density surface, an Eulerian section of PV across the stream was constructed from the above; that is, $\text{PV}(x)$ for a specific ρ was extracted from $\text{PV}(x, \rho)$.

The origin of the cross-stream coordinate x was chosen as the point of intersection of an isopycnal and a convenient, arbitrary depth (e.g., $x = 0$ at the intersection of $\sigma_\theta = 26.5$ crossing 150 m). This definition of the alongstream axis is an operational one since the stream as a whole undergoes adjustments when it meanders and there is no fixed downstream axis in the current around which everything else adjusts.

Cross-trajectory and cross-stream distances measured with respect to density structure at any given point on the parcel's trajectory are nearly equal since the angle between the trajectory and streamlines is very small in the upper thermocline [e.g., for our study, this angle (α), was less than $1^\circ\text{--}3^\circ$ ([Fig. 2](#))]. It should be noted, however, that it is this small angle that causes the deviation of the trajectory from the streamlines and the lateral motion of the parcel. While the difference between the cross-stream and cross-trajectory distances, measured respectively in the cross-stream and cross-trajectory directions, depends on $\cos \alpha$ (which tends to 1 for small α), the lateral motion of the parcel across the stream depends on $\tan \alpha$ (which tends to α for small α). Therefore, cross-stream displacement of the particle and cross-trajectory displacement of the particle will be used interchangeably, here.


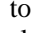
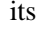
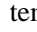
Uncertainties in velocity and density measurements will cause errors in the above calculations. This error was estimated with the bootstrap method ([Efron and Gong 1983](#)) by generating different ensembles of data from the observed realization. Different velocity ensembles were generated by adding a random normal noise with a standard deviation of 1 cm s^{-1} to the velocity data measured by the ADCP. Internal waves constantly perturb the isopycnals and could have caused errors in


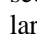
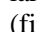
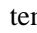
instantaneous estimate of layer thickness from CTD measurements. Various ensembles of CTD data were simulated by the addition of random normal noise with a standard deviation of 5 m to the depths from the CTD casts. This noise was not correlated vertically or horizontally and, therefore, represents a worse-than-real case since in reality the isopycnal displacements under the influence of internal waves may be correlated over some vertical distance. The choice of 5 m as the standard deviation was based on the observed amplitude of the internal waves from the pressure sensors on the isopycnal floats tagging parcels F1 and F2. For a hundred simulated ensembles, standard error bars (68% confidence intervals on the mean) on the values of $PV(x, \rho)$ were determined as the 16th and 84th of the sorted values. Also, uncertainties in the measurement of density caused by the internal waves would cause uncertainties in the location of the origin of the cross-stream coordinate x . By using the 100 ensembles mentioned above, the error in the mean position of the origin was estimated at 100–500 m for the various cross-stream transects. These errors were considered small compared to the $O(10\text{ km})$ cross-stream spans of the transects.

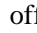
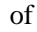
3. Results

Five water parcels on the isopycnal $\sigma_\theta = 26.6$, in the upper thermocline, were tracked during this Lagrangian study of evolution of the PV field at the northern edge of the Gulf Stream. The results of three of these studies are presented as case studies below; they elaborate and emphasize the principal features of the observations. The results from all the parcels are then summarized in [section 3b](#).

a. Case studies

Parcel F2 was tracked upstream of a meander crest on the cyclonic side. From the velocity and density fields measured around the parcel, it can be seen that it upwelled, slowed down, and moved onshore while approaching the crest ([Fig. 3](#) ). The depth of the parcel was determined from the measured cross-stream density sections of the stream and the known position of the parcel in these sections. The speed of the parcel was calculated by first-differencing the trajectory of the parcel with respect to time. The lateral motion of the parcel was determined from the known position of the parcel in the density sections with respect to an arbitrary origin, defined as $\sigma_\theta = 26.5$ crossing 150 m. These records show that, as the parcel approached the crest, it shoaled by 50 m, lost about 30% of its original speed, and moved onshore by 8.5 km. During this time, the PV cross sections of the stream in the vicinity of the parcel determined from the CTD and ADCP data show it to be embedded in a large PV gradient ([Fig. 4](#) ). The dashed lines on the left y axis of each panel are the limiting values of slope waters and Sargasso Sea potential vorticities, calculated as f/H , where H is a typical layer thickness at $\sigma_\theta = 26.6$. The value of H for the Sargasso Sea was obtained from [Leaman et al. \(1989\)](#), who report layer thicknesses on various isotherms across the stream. The layer thickness values from this source could not be used to get H on $\sigma_\theta = 26.6$ for the slope waters since (i) temperature and density are not correlated on the slope waters as they are in the Sargasso Sea and (ii) seasonal and interannual signals exist at the shallow depths of $\sigma_\theta = 26.6$ on the slope water side but not on the Sargasso Sea side of the stream where this isopycnal is much deeper. The value of H used for slope water PV was the depth difference between isopycnals $\sigma_\theta = 26.4$ and 26.8 from a CTD cast during the fall cruise (same cruise as F1 and F2) in the slope waters. It should be noted that the slope water PV was calculated based on a single CTD cast and should therefore be considered only as a reference value. The parcel F2 moved across the stream in the presence of a cross-stream PV front but did not undergo any significant change in its Lagrangian PV. This can be explained by the observed cross-stream migration of the PV front itself. During the course of two days, the PV front around the parcel shifted about 8 km onshore ([Fig. 4](#) ). The temperature of the parcel (curves on the lower half of the panels in [Fig. 4](#) , with tickmarks on the right y axis) increased by about 0.8°C during this period, which will be discussed in greater detail in the next section.

Parcel F1 was also tracked upstream of a meander crest on the cyclonic side. From the velocity and density fields measured around the parcel, it can be seen that it upwelled, slowed, and moved onshore while approaching the crest ([Fig. 5](#) ). The depth, speed, and lateral motion of the parcel were determined as explained in the previous paragraph. These records (especially the velocity) document the ejection of the parcel from the high-speed core of the stream, during which it shoaled more than one-third of its original depth and lost more than 80% of its original speed. During this time, the PV cross sections of the stream in the vicinity of the parcel determined from the CTD and ADCP data show it to be embedded in a large PV gradient ([Fig. 6](#) ). During the course of the first day, the PV front around the parcel shifted about 8 km onshore (first four panels of [Fig. 6](#) ). As the parcel moved farther onshore into the high-shear edge of the stream, the PV front was less prominent; it has probably begun to diffuse, aided by the high horizontal shear and the low advection. The temperature of the parcel (curve on lower half of the panels in [Fig. 6](#) ) dropped by about 0.5°C during its detrainment from the stream into the colder slope water, which will be discussed in greater detail in the next section.

A water parcel P3, tracked with the ADCP during the late-spring cruise, was absorbed into the stream from the slope waters downstream of a meander crest. The parcel downwelled from 90 to 135 m, increased its speed threefold, and moved offshore by about 8 km during the process of entrainment ([Fig. 7](#) ). Again the parcel can be seen as embedded in regions of rapidly changing PV throughout this process, although it does not significantly change its Lagrangian PV ([Fig. 8](#) ). As before, it was the cross-stream migration of the cross-stream PV structure itself that facilitated the parcel to move across

the stream without changing its PV by as much as would be expected from the surrounding PV structure. The temperature of the parcel (curve on lower half of the panels in Fig. 8) did not change significantly as it was absorbed into the stream. The limiting PV values for the slope waters and the Sargasso Sea in Fig. 8 were taken as the same as in the fall cruise, though the slope water value may have been different during this spring cruise.

b. Summary of results

The lateral motion of parcels in the stream was consistent with previous observations (e.g., Bower 1989) onshore (offshore) upstream(downstream) of a crest and offshore(onshore) downstream(upstream) of a trough. However, it should be noted that previous float studies in the stream did not consider parcels leaving or entering the stream and assumed that Lagrangian PV was conserved. Of the five parcels tracked, F1 was almost ejected from the stream upstream of a crest and P3 was absorbed into the stream downstream of a crest as discussed in the previous section. From the late-spring cruise, P1 first moved offshore and then onshore as it negotiated a meander trough, undergoing downwelling and upwelling in turn (Table 1). Parcels P2 from the same cruise and F2 from the early fall cruise were tracked as they approached a meander crest, moved onshore, and continued to flow down the stream without being ejected (Table 1). As seen for the three cases above, when a water parcel moved laterally across the stream, its Lagrangian PV of the parcel did not change significantly (except at the high-shear onshore edge), while the Eulerian PV section around the parcel underwent considerable evolution. A parcel can move across the stream while conserving its PV because the cross section of the PV front itself moves across the stream.

These five cases differ in many respects such as the amount of tracking time, the radius of curvature of the meander, and the cross-stream position of the parcel, which determine how a given parcel moves laterally. In order to compare the various cases, these variables were combined in an integrated sense as $\theta_{av} = \int \kappa \mathbf{v} dt$, where κ is the curvature of the trajectory, \mathbf{v} is the velocity of the parcel, and the integration is carried out over the time the parcels were tracked. The velocity of the parcel was used as a proxy for its cross-stream position so that this integral can be used in a general case where simultaneous hydrography is not available to determine the parcel's cross-stream position. This nondimensional integral can be thought of as the angular distance covered by the parcel in a given time interval. This integral measure, θ_{av} , and the average value of curvature along the trajectory of a parcel (κ_{av} in Table 1) would help us compare the various parcel cases by placing them on equivalent arcs of concentric circles (Fig. 9). Also, it was observed that the absolute value of the cumulative cross-frontal displacement ($\int \Delta x$, measured as the distance from a reference isobar to the parcel's position, in the direction perpendicular to the parcel trajectory) bore an apparent linear relationship with the absolute value of the quantity $\theta_{av}^2 / \kappa_{av}$ (where $\theta_{av} = \int \kappa dl$), which can be interpreted as the centrifugal force integrated twice with respect to time (appendix B). Although only five parcels were tracked, the many points that indicate this linear relationship (Fig. 10) were generated by carrying out the integration over various intermediate intervals of the individual parcel tracks. Though such a linear relationship is plausible (appendix B), it is not clear why the slope of the line is close to 0.1. It should also be noted that the centrifugal force and $\int \Delta x$ were measured in the same direction, perpendicular to the trajectory. See appendix B for details.

The most striking result of this study was that the PV fields in the vicinity of the parcels were observed to migrate in the cross-stream direction and evolve, as the parcels moved laterally on the isopycnal (Fig. 6 for F1, Fig. 8 for P3, and Fig. 4 for F2). As a result of this, changes in Lagrangian potential vorticity (LPV) of parcels as they moved laterally on isopycnals were much smaller than the ambient change in Eulerian PV over a distance comparable to the lateral migration of the parcels (Table 1).

4. Discussion

a. Significance of the cross-stream migration of the PV front

The strong PV front observed to be aligned with the cyclonic side of the upper thermocline in the current (e.g., Bower and Lozier 1994) has been thought of as a fixed “barrier” that inhibits lateral motion in the stream. It has been suggested that conservation of PV is a dynamic constraint that controls the depth-dependent exchange across the Gulf Stream and that this exchange is inhibited in the upper layer due to the existence of a strong PV front (Bower et al. 1985; Lozier and Riser 1990). Bower and Lozier (1994) state that the strong PV front associated with the midlatitude jet appears to restrict particles from crossing out of the stream.

Traditionally, the particles in the stream were thought to move laterally in the stream only until they encounter the PV front, the cross-stream position of which was perceived as fixed. The current study, however, shows not only that the PV front in the stream moves laterally, but also that the magnitude of the lateral motion of the PV front is of the same order as the lateral motion of the particles. Thus, the traditional idea of the role played by the PV front in inhibiting the lateral motion of the particles in the stream needs to be revised.

With respect to the density structure, the lateral motion of the particles is much greater than any lateral motion of the velocity structure. This is obvious from the fact that, when parcels move across the stream in a meander, they rapidly change velocity (observed in this and previous studies; [Figs. 3, 5, 7](#)); it can also be seen from cross sections of velocity (not shown) constructed at various downstream locations, during this study. The magnitude of the lateral shift of the PV front was comparable to that of the particles, that is, much greater than the shift of the velocity structure (all shifts measured with respect to the density structure). From this point of view, the role of the PV front is not to inhibit the parcel motion; on the other hand, the lateral motion of the front is a response to the lateral motion of the parcels and to the adjustment process associated with the meandering of the stream.

The particles that make up the front, on either side of the Lagrangian particle of interest, are different at different downstream cross sections due to the horizontal shear in the stream. Therefore, the observed lateral motion of the PV front is not a simple cross-stream translation of the front.

It should be noted that, while the PV front was observed to move laterally across the stream, away from the velocity maximum and farther onshore (with respect to the density structure), it cannot be thought to move out of the velocity envelope of the stream itself. The presence of a PV front requires a rapid change in velocity shear or a rapid change in layer thickness (which would be accompanied by large geostrophic velocity), neither of which are possible outside the velocity envelope of the stream, except in the case of streamers ([Hitchcock et al. 1994](#)). The onshore lateral motion of the PV front allows parcels to move across the stream without changing their LPV or crossing the PV front, until the motion of the front is constrained by the edge of the stream. Once near the edge of the velocity envelope of the stream, the parcel can move farther onshore only by changing its LPV since the Eulerian PV front cannot move onshore any more. In the low-velocity, high-shear regime of the onshore edge, PV diffuses with the surroundings, especially since the high shear stretches material patches and increases property gradients. This would change the LPV of the parcel and cause the Eulerian PV front to evolve. As an example, consider the increasing LPV of parcel F1 (changing position of the tick mark on the left y axes in the panels of [Fig. 6](#)) as it slows down at the edge of the stream, which is accompanied by an evolution of the Eulerian PV front (the flattening of the PV curve and its approach to the slope water values in successive panels of [Fig. 6](#)). As the parcels at the edge of the stream attain the PV of the slope waters by diffusion, the PV front would relax to the offshore side of these parcels between regimes of slope water PV and stream PV.

The traditional ideas that the PV front inhibits lateral exchange and that it restricts exchange needs to be revised because (i) in the presence of a PV front, parcels in the stream were observed to move across the stream without significantly changing PV since the PV itself moved by a comparable distance and (ii) parcel F1 was observed to mix its PV up to the slope water value in the high-shear edge regime and exit the stream.

Another significance of the observed migration of the PV front may be in its application to numerical models that use a typical PV cross section to initialize the stream. Given that PV fronts $O(10 \text{ km})$ were found to migrate across the stream by $O(10 \text{ km})$ in the meanders, a PV section that depends on curvature may be more appropriate than a typical PV section in stream initialization.

b. Components of PV


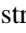
In the Eulerian sections taken around parcels, the contributions of various PV components to the change in PV across the sections were investigated by differentiating [Eq. \(1\)](#) as

$$\begin{aligned} \frac{dPV}{PV} = & \frac{df}{f + \frac{\partial v}{\partial n} + \kappa v} + \frac{d\left(\frac{\partial v}{\partial n}\right)}{f + \frac{\partial v}{\partial n} + \kappa v} \\ & + \frac{d(\kappa v)}{f + \frac{\partial v}{\partial n} + \kappa v} - \frac{dH}{H}. \end{aligned} \quad (3)$$

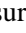
The contributions by changes in planetary and curvature vorticities across the sections [first and third terms respectively on the right-hand side of [Eq. \(3\)](#)] to the increase in PV toward the slope waters were much smaller than the contributions by changes in shear and stretching [second and fourth terms respectively on the right-hand side of [Eq. \(3\)](#)]. The percentage contributions of changes in shear and stretching to shoreward PV increase across the sections were different for sections taken around different parcels ([Table 1](#)). In the sections around parcel F1, the increase of Eulerian PV toward slope

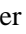

waters was due to the large increase in stretching vorticity that more than offset the decrease in shear across the sections. In the sections around parcels F2 and P2, increase in stretching toward the shore was responsible for the increase in Eulerian PV, while shear did not change much across the sections. Shear and stretching contributed equally to Eulerian PV increase across sections around parcel P3. Increase in Eulerian PV in the sections around parcel P1 was due to increase in shear; stretching did not change much across these sections. Thus, these observations show that the PV front in the upper thermocline could be the result of rapid change in shear, stretching, or both.

A section of the frozen-field stream (Halkin and Rossby 1985) would lead us to expect layer thickness decrease (or stretching vorticity increase) toward the shore along all sections of the stream. The frozen-field velocity sections on the cyclonic side of the stream show a region of decreasing shear toward the shore at the onshore edge of the stream and another of increasing shear offshore of it, closer to the velocity maximum (e.g., Fig. 2b of Bower 1989). When compared to this frozen-field stream, our observations show a richer structure in terms of combinations of changes in shear and stretching across the stream, which is similar to the patchiness and smaller-scale structures in the velocity and vorticity sections of the stream observed by Liu and Rossby (1993).

In the cases where the Lagrangian PV of the parcels were observed to change, there was an increase in PV for upwelling parcels and a decrease in PV for downwelling parcels (Table 1 ) , consistent with the fact that slope waters have greater PV than the stream. For these cases, the change in PV components and their contribution to the change in PV were estimated based on Eq. (5) (Table 1 ) . Changes in shear and stretching contributed in varying extents to the change in Lagrangian PV of the parcels, while the changes in planetary and curvature vorticities were much smaller in comparison. As parcel F1 upwelled, increasing stretching vorticity more than compensated for decreasing shear and raised the LPV of the parcel. For parcel F2, increasing stretching and shear resulted in increasing LPV when it upwelled. While parcel P1 downwelled, its shear and stretching vorticities decreased to lower its LPV and, while it upwelled, its shear and stretching vorticities increased to raise its LPV. Parcels P2 and P3 did not change their LPV significantly.

c. Stirring and mixing

While tracking parcel F2, stirring of fresh cool waters into the stream was observed in the cross-stream temperature signal on the parcel's isopycnal (Fig. 4 ) . This subsurface equivalent of surface streamers was manifest in the $O(5\text{ km})$ wiggles of temperature on the isopycnal.

Due to the nonlinear dependence of density on temperature and salinity, different water masses on an isopycnal cannot be easily discerned by differences in their salinities or temperatures alone. An efficient descriptor of different water masses on a given isopycnal is τ (Veronis 1972), which combines temperature and salinity into a single variable. It is computed as a variable orthogonal to σ_θ in the θ - S plane and is dynamically passive. Different values of τ on an isopycnal would indicate the presence of different water types, while uniform τ on an isopycnal indicates complete mixing. Contours of τ at various cross sections of the stream show the intrusion of freshwater into the stream (Fig. 11 ) shows this for sections around F2). Lower τ values correspond to the cooler fresher water and higher τ values to warmer saltier stream water. While the upper sides of the lens of cool fresh intrusion into the stream would be conducive to salt fingering, the lower sides would be conducive to diffusive convection. In the sections approaching a crest, most of the upper 200 m is conducive to salt fingering since warm stream water overlies colder fresher water. Against this general background, lenses of freshwater trapped in the stream can be seen in each section (Fig. 11 ) , starting at the lower left corner and extending diagonally across each panel. Together, these sections indicate a long filament of fresher water in the stream, with a cross-stream width of about 10 km. It is possible that these fresher waters are Ford waters that originate on the shelf (Ford et al. 1952), given that their salinity is 35.6–35.8 psu and their temperature is 14°–16°C.


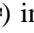
Closely packed tau lines along an isopycnal indicate a strong property gradient. While the type of double diffusive process would be determined by the relative positions of warm salty water and cold fresher water, a quantitative idea of mixing can be had from how closely packed the tau lines are. As these filaments get stretched in the alongstream direction and squeezed in the cross-stream direction by the large lateral velocity shear, diffusion will become stronger and finally mixing will erase the gradients. The observational period of this study, however, did not cover the complete mixing process.


Diffusivities for temperature were investigated based on the observed changes in parcel properties and ambient spatial gradient of the properties. For temperature, when all mixing was assumed to be vertical (i.e., $DT/Dt = \kappa_V \partial^2 T / \partial z^2$) the required vertical diffusivity was $O(10^{-4} - 10^{-3} \text{ m}^2 \text{ s}^{-1})$, much higher than the canonical value of $10^{-5} \text{ m}^2 \text{ s}^{-1}$ (e.g., Gregg and Sanford 1980). This probably means that horizontal mixing is the main mechanism of mixing. If we instead assume only lateral mixing (i.e., $DT/Dt = \kappa_H \partial^2 T / \partial x^2$, where x is the cross trajectory coordinate), we obtain a horizontal diffusivity of $O(10 - 10^3 \text{ m}^2 \text{ s}^{-1})$.

Potential vorticity diffusivities were also investigated starting with

$$\frac{DPV}{Dt} = A_H \frac{\partial^2 PV}{\partial x^2} + A_V \frac{\partial^2 PV}{\partial z^2},$$

which is satisfied if density is conserved. When it was assumed that $A_H = 0$, A_V was estimated to be $O(10^{-2} \text{ m}^2 \text{ s}^{-1})$ —again a value much higher than canonical values, which means that here too the main mechanism of mixing is horizontal. When all mixing was considered to be horizontal, A_H was estimated to be $O(10-10^2 \text{ m}^2 \text{ s}^{-1})$.

Changes in the temperature of tracked water parcels were associated with interleaving processes, as seen from CTD casts in the region. Over the course of two days, F2 increased its temperature by almost 1°C while approaching a crest and moving onshore. Interleaving processes were observed in the CTD casts taken at the parcel during this time. This interleaving was visible in the θ - S plots and in the plots of τ at various sections of the stream near the parcel. The increase in temperature of this parcel as it moves onshore was contrary to our expectation of a reduction in temperature when a parcel of stream water mixes with the slope waters. The reason for this increase turns out to be that the float was launched in cool fresher waters that had intruded into the stream. This intrusion can be seen as a lens in the τ contours (Fig. 11 ) , where the fresher water with lower τ values at the onshore edge of each section is surrounded by stream water with higher τ values. The τ value at the location of the parcel (intersection of $\sigma_\theta = 26.6$ and vertical dashed line in Fig. 11 ) increased and the lens of intrusion became less prominent at cross sections farther downstream, as the fresher water mixed into the surrounding stream.

As F1 approached a crest, its temperature fell by 0.4°C over the first day (Fig. 6 ) . This decrease in temperature was associated with intrusive features observed at the float. Contours of τ and θ - S plots from CTD casts showed much weaker property gradients around this parcel than for F2, consistent with the lower magnitude of temperature change for F1 compared to F2.

The three water parcels tracked during the late-spring cruise did not show much change in temperature and there was very little interleaving in their neighborhood, though these parcels too were launched in the upper main thermocline on the cyclonic side of the stream and in the same geographic region as the floats in the early fall cruise. Perhaps the intrusion of cooler fresher water into the stream is a seasonal event, but the data do not suffice to address this issue. What can be concluded, however, is that observed changes in temperature were concurrent with observed interleaving events.

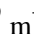
d. Diapycnal mixing

When Lagrangian PV is conserved, any change in absolute vorticity must be balanced by epipycnal divergence/convergence:

$$\begin{aligned} \frac{1}{PV} \frac{DPV}{Dt} &= \frac{1}{H} \frac{DH}{Dt} + \frac{1}{\zeta_a} \frac{D\zeta_a}{Dt} \\ &= \left(\frac{\partial u}{\partial x} + \frac{\partial v}{\partial y} \right) + \frac{1}{\zeta_a} \frac{D\zeta_a}{Dt} = 0, \end{aligned} \quad (4)$$

where x and y are measured along the isopycnal. In the presence of diapycnal mixing, $H^{-1}DH/Dt$ would be expanded as $(\partial u/\partial x + \partial v/\partial y + \partial w_\rho/\partial \rho)$, where w_ρ is the diapycnal velocity and $\partial w_\rho/\partial \rho$ is the diapycnal convergence/divergence. Assuming that all of the observed change in Lagrangian PV in our measurements results from diapycnal convergence/divergence (i.e., ignoring lateral mixing), we can write

$$\frac{1}{PV} \frac{DPV}{Dt} = \frac{\partial w_\rho}{\partial \rho}. \quad (5)$$

An upper limit on diapycnal convergence/divergence can then be estimated by considering the extreme case of a parcel changing its PV from a value typical to the Sargasso Sea to a value typical to the slope waters over $O(2 \text{ days})$, a typical timescale for entrainment/detrainment process in the upper thermocline. By using a mean PV value of $1 \times 10^{-9} \text{ m}^{-1} \text{ s}^{-1}$ and a change in PV of the same order (between the two limits shown in dashed lines in Figs. 4, 6, and 8 ) over 2 days, the upper limit on $\partial w_\rho/\partial \rho$ is $5 \times 10^{-6} \text{ s}^{-1}$ from Eq. (5). Our estimate of $\partial w_\rho/\partial \rho$ is likely an overestimate since it is based on the assumption of mixing being exclusively vertical, while the discussion in the previous section suggests that horizontal mixing

is more important than vertical mixing.

This estimate is much lower than $5 \times 10^{-4} \text{ s}^{-1}$ reported by [Pelegri and Csanady \(1994\)](#), based on the assumption that mixing is due to shear instability and a maximum eddy diffusivity of $4 \times 10^{-4} \text{ m}^2 \text{ s}^{-1}$ for unstable conditions. From our measurements of density and velocity in the vicinity of the parcel, a few patches with Richardson numbers (Ri) of $O(1)$ were discerned in the upper thermocline. Although Ri values less than 0.25 were not observed, the $O(1)$ values may be indicative of shear instability since velocity was measured with 8-m bins for the ADCP. Perhaps the larger estimate by [Pelegri and Csanady \(1994\)](#) resulted from their choice of eddy diffusivity.

5. Summary

Parcels observed to move laterally in Gulf Stream meanders conserved Lagrangian PV while they remained within the stream. The PV front associated with the stream moved laterally by nearly the same extent as the parcels themselves. In the high-shear environment of the stream, the observed cross-stream motion of the PV front is not a simple cross-stream translation of the front. The lateral motion of the parcels and the PV front was much greater than the lateral motion of the velocity structure in the meandering stream. These observations suggest that the traditional idea of the PV front as inhibiting the lateral motion needs to be revised. Although parcels were observed to move laterally in the stream, conserving their PV, once the edges of the stream constrain the lateral motion of the PV front, the parcel moves further laterally by changing its Lagrangian PV, as observed in the case of a parcel that exited the stream.

Changes in shear and stretch vorticity were in general more important to the cross-stream PV gradient than changes in planetary or curvature vorticity. The observed combinations of changes in shear and stretching across the stream reveal a richer structure than that expected from a frozen-field stream. In the cases of observed Lagrangian PV changes also, changes in shear and stretching dominated changes in planetary and curvature vorticities.

Cool fresh subsurface waters intruded into the meanders around the parcels; observed temperature changes of parcels were associated with these intrusions. Diffusivities calculated from observed parcel property changes indicate that the main mechanism of mixing is horizontal rather than vertical in the upper thermocline of the stream. Typical timescales of entrainment/detrainment processes and associated changes in Lagrangian PV also suggest that diapycnal mixing is small in the upper thermocline of the stream.

Acknowledgments

We thank Jim Fontaine and Mark Prater for the preparation and operation of the floats and Sandy Anderson-Fontana for processing the ADCP data. We are grateful to the masters, crew, and technicians of R/V *Endeavor* and R/V *Oceanus* and to all those who stood watches during the two cruises. We thank Randy Watts and Paula Perez-Brunius for helpful comments. This manuscript has benefited greatly from the comments by two reviewers. This work was supported by Grant OCE 9314480 from the National Science Foundation and the State of Rhode Island and Providence Plantations.

REFERENCES


- Bower A. S., 1989: Potential vorticity balances and horizontal divergence along particle trajectories in Gulf Stream meanders east of Cape Hatteras. *J. Phys. Oceanogr.*, **19**, 1669–1681. [Find this article online](#)
- Bower A. S., 1991: A simple kinematic mechanism for mixing fluid parcels across a meandering jet. *J. Phys. Oceanogr.*, **21**, 173–180. [Find this article online](#)
- Bower A. S., and H. T. Rossby, 1989: Evidence of cross-frontal exchange processes in the Gulf Stream based on isopycnal RAFOS float data. *J. Phys. Oceanogr.*, **19**, 1177–1190. [Find this article online](#)
- Bower A. S., and M. S. Lozier, 1994: A closer look at particle exchange in the Gulf Stream. *J. Phys. Oceanogr.*, **24**, 1399–1418. [Find this article online](#)
- Bower A. S., H. T. Rossby, and J. T. Lillibridge, 1985: The Gulf Stream—Barrier or blender? *J. Phys. Oceanogr.*, **15**, 24–32. [Find this article online](#)
- Efron B., and G. Gong, 1983: A liesurly look at the bootstrap, the jackknife, and cross-validation. *Amer. Stat.*, **37**, 36–48. [Find this article online](#)
- Ford W. L., J. R. Longrad, and R. E. Banks, 1952: On the nature, occurrence and origin of cold low salinity water along the edge of the Gulf Stream. *J. Mar. Res.*, **11**, 281–293. [Find this article online](#)

- Gregg M. C., and T. B. Sanford, 1980: Signatures of mixing from the Bermuda Slope, Sargasso Sea and the Gulf Stream. *J. Phys. Oceanogr*, **10**, 105–127. [Find this article online](#)
- Halkin D., and T. Rossby, 1985: The structure and transport of the Gulf Stream at 73°W. *J. Phys. Oceanogr*, **15**, 1439–1452. [Find this article online](#)
- Hitchcock G. L., T. Rossby, J. L. Lillibridge III, E. J. Lessard, E. R. Levine, D. N. Connors, K. Y. Borsheim, and M. Mork, 1994: Signatures of stirring and mixing near the Gulf Stream front. *J. Mar. Res*, **52**, 797–836. [Find this article online](#)
- Holland W. R., and P. B. Rhines, 1989: An example of eddy-induced ocean circulation. *J. Phys. Oceanogr*, **10**, 1010–1031. [Find this article online](#)
- Hummon J., 1995: A Gulf Stream–warm core ring interaction—Case study using statistical optimal interpolation. Ph.D. dissertation, Graduate School of Oceanography, University of Rhode Island, 181 pp.
- Lai D., and P. Richardson, 1977: Distribution and movement of Gulf Stream rings. *J. Phys. Oceanogr*, **7**, 670–683. [Find this article online](#)
- Leaman K. D., E. Johns, and T. Rossby, 1989: The average distribution of volume transport and potential vorticity with temperature at three sections across the Gulf Stream. *J. Phys. Oceanogr*, **19**, 36–51. [Find this article online](#)
- Lillibridge J. L., and J. M. Hummon, 1990: Hydrographic and kinematic changes in Gulf Stream meanders during ring–stream interaction. *Extended Abstracts, Ocean Science Meeting*, New Orleans, LA, Amer. Geophys. Union, 188 pp.
- Liu M., and T. Rossby, 1993: Observations of the velocity and vorticity structure of Gulf Stream meanders. *J. Phys. Oceanogr*, **23**, 329–345. [Find this article online](#)
- Lozier M. S., and S. C. Riser, 1989: Potential vorticity dynamics of boundary currents in a quasi-geostrophic ocean. *J. Phys. Oceanogr*, **19**, 1373–1396. [Find this article online](#)
- Lozier M. S., and S. C. Riser, 1990: Potential vorticity sources and sinks in a quasi-geostrophic ocean: Beyond western boundary currents. *J. Phys. Oceanogr*, **20**, 1608–1627. [Find this article online](#)
- Lozier M. S., L. J. Pratt, A. M. Rogerson, and P. D. Miller, 1997: Exchange geometry revealed by float trajectories in the Gulf Stream. *J. Phys. Oceanogr*, **27**, 2327–2341. [Find this article online](#)
- Owens W. B., 1984: A synoptic and statistical description of the Gulf Stream and subtropical gyre using SOFAR floats. *J. Phys. Oceanogr*, **14**, 104–113. [Find this article online](#)
- Pelegri J. L., and G. T. Csanady, 1994: Diapycnal mixing in western boundary currents. *J. Geophys. Res*, **99**, 18275–18304. [Find this article online](#)
- Rajamony J., D. Hebert, S. Fontana, and T. Rossby, 1997: Data report for “Dynamical Adjustment along Gulf Stream Trajectories” cruises (OC267 and EN272). University of Rhode Island GSO Tech. Rep. 91-5, 161 pp.
- Rajamony J., D. Hebert, and T. Rossby, 1999: Estimating Lagrangian trajectory with an ADCP. *J. Atmos. Oceanic Technol*, **16**, 1255–1263. [Find this article online](#)
- Schmitz W. J., and M. S. McCartney, 1993: On the North Atlantic circulation. *Rev. Geophys*, **31**, 29–49. [Find this article online](#)
- Song T., and T. Rossby, 1997: Analysis of Lagrangian potential vorticity balance and lateral displacement of water parcels in Gulf Stream meanders. *J. Phys. Oceanogr*, **27**, 325–339. [Find this article online](#)
- Song T., T. Rossby, and E. Carter, 1995: Lagrangian studies of fluid exchange between the Gulf Stream and the surrounding waters. *J. Phys. Oceanogr*, **25**, 46–63. [Find this article online](#)
- Veronis G., 1972: On properties of seawater defined by temperature, salinity, and pressure. *J. Mar. Res*, **30**, 227–255. [Find this article online](#)
- Yang H., 1996a: Chaotic transport and mixing by ocean gyre circulation. *Stochastic Modelling in Physical Oceanography*, R. J. Adler, P. Müller, and B. L. Rozovskii, Eds., Birkhäuser, 439–466.
- Yang H., 1996b: The subtropical/subpolar gyre exchange in the presence of annually migrating wind and a meandering jet: Water mass exchange. *J. Phys. Oceanogr*, **26**, 115–130. [Find this article online](#)


6. Components of Potential Vorticity

The expression for Ertel's PV ($\zeta_a \cdot -\nabla\rho/\rho$) can be related to the planetary, curvature, shear, and stretching vorticities as follows. In a northeast coordinate system, Ertel's PV can be written as

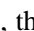
$$\zeta_a \cdot \frac{\nabla\rho}{\rho} = \left(\frac{\partial w}{\partial y} - \frac{\partial v}{\partial z} \right) \frac{1}{\rho} \frac{\partial\rho}{\partial x} + \left(\frac{\partial u}{\partial z} - \frac{\partial w}{\partial x} \right) \frac{1}{\rho} \frac{\partial\rho}{\partial y} + \left(f + \frac{\partial v}{\partial x} - \frac{\partial u}{\partial y} \right) \frac{1}{\rho} \frac{\partial\rho}{\partial z}.$$

Now, in the Gulf Stream, the horizontal shear of the vertical velocity (terms $\partial w/\partial x$ and $\partial w/\partial y$) is several orders of magnitude smaller than the vertical shear of the horizontal velocities (terms $\partial u/\partial z$ and $\partial v/\partial z$). Therefore, the expression for PV in the Gulf Stream in a geographical coordinate system (top panel of [Fig. A1](#) ) is

$$\text{PV} = -\frac{\partial v}{\partial z} \frac{1}{\rho} \frac{\partial\rho}{\partial x} + \frac{\partial u}{\partial z} \frac{1}{\rho} \frac{\partial\rho}{\partial y} + \left(f + \frac{\partial v}{\partial x} - \frac{\partial u}{\partial y} \right) \frac{1}{\rho} \frac{\partial\rho}{\partial z}.$$

In a natural coordinate system (middle panel of [Fig. A1](#) ) , where x is the across the stream, y is the alongstream, and z is vertical, the above equation becomes

$$\text{PV} = -\frac{1}{\rho} \frac{\partial\rho}{\partial x} \frac{\partial v}{\partial z} + \frac{\partial\rho}{\partial z} \left(f + \frac{\partial v}{\partial x} + \kappa_s v \right), \quad (\text{A1})$$

where $\kappa_s v$ is the curvature vorticity. This is the same as [Eq. \(2\)](#) in [section 2a](#). The x and z axes may now be rotated through an angle α so that the cross-stream axis is tangential to the isopycnal while z is perpendicular to it (bottom panel of [Fig. A1](#) ) . Since the slope of the isopycnals across the Gulf Stream is $O(0.01)$, the values of planetary vorticity and vertical stratification in the rotated frame may be taken as the same as in the natural coordinate system and PV may be written as

$$\text{PV} = \frac{1}{\rho} \frac{\partial\rho}{\partial z} \left(f + \frac{\partial v}{\partial n} + \kappa_s v \right), \quad (\text{A2})$$

where n is the cross-stream coordinate along the isopycnal. This is the same as [equation \(1\)](#) in [section 2](#), if H —separation between isopycnals—is used instead of $(\rho^{-1}\partial\rho/\partial z)^{-1}$. Shear vorticity, $\partial v/\partial n$, is a measure of the cross-stream shear, while curvature vorticity, $\kappa_s v$, is a measure of the rotation of the cross-stream axis with respect to the geographic coordinates. The sum of shear and curvature vorticities is the relative vorticity of the parcel.

Also, [Eq. \(A1\)](#) may be rewritten as

$$\text{PV} = \frac{1}{\rho} \frac{\partial\rho}{\partial z} \left(\frac{-\frac{1}{\rho} \frac{\partial\rho}{\partial x} \frac{\partial v}{\partial z}}{\frac{1}{\rho} \frac{\partial\rho}{\partial z}} + f + \frac{\partial v}{\partial x} + \kappa_s v \right)$$

so that by comparison with [Eq. \(A2\)](#) it can be seen that shear vorticity $\partial v/\partial n$ in the rotated coordinate system is the same as

$$\left(-\frac{1}{\rho} \frac{\partial \rho}{\partial x} \frac{\partial v}{\partial z} / \frac{1}{\rho} \frac{\partial \rho}{\partial z} \right) + \frac{\partial v}{\partial x}$$

in the natural coordinate system.

APPENDIX B

7. Lateral Motion of Parcels in Meanders

The lateral motion of parcels in the meanders, across isobars on a given isopycnal, is related to the imbalance among the centrifugal force, the Coriolis force, and the pressure gradient. That is, near a crest, if the centrifugal force is greater than the difference between the pressure gradient and the Coriolis force, the parcel moves onshore and vice versa. In the steady case, where streamlines coincide with particle trajectories, the balance would be

$$\kappa v^2 - fv = \frac{-1}{\rho} \frac{\partial p}{\partial x},$$

where x is the cross-trajectory direction and y is the along-trajectory direction. If we assume that the lateral displacement Δx is caused by the imbalance among the forces, then


$$\Delta x = \iint \left(\kappa v^2 - fv + \frac{1}{\rho} \frac{\partial p}{\partial x} \right) dt dt,$$

i.e.,

$$\Delta x = \iint \kappa v^2 dt dt + \iint \left(-fv + \frac{1}{\rho} \frac{\partial p}{\partial x} \right) dt dt. \quad (B1)$$

The variable $\theta_{av}^2/\kappa_{av}$ used in [section 3b](#), where $\theta_{av} (= \int \kappa dl)$ and κ_{av} are average integrated values, can be related to $\iint \kappa v^2 dt dt$ as follows:

$$\kappa v^2 \Delta t \Delta t = \kappa \Delta l \Delta l = \frac{(\Delta \theta)^2}{\kappa}. \quad (B2)$$

[Equations \(B1\) and \(B2\)](#) suggest the relation between centrifugal acceleration integrated twice with respect to time and cumulative lateral displacement, or the relation between θ^2/κ and x . However, it is not clear why this relationship should be near linear ([Fig. 10](#) .

Tables

TABLE 1. Comparison of cross-stream motion of parcels. Lateral motion (Δx) of various parcels (–ve onshore, +ve offshore), typical ambient Eulerian cross-stream PV change corresponding to this Δx , the change in Lagrangian PV (where zero denotes no significant change), and the time for which each parcel was tracked. The contributions of stretching and shear vorticities to the Eulerian and Lagrangian PV changes are shown as percentages (see text for explanation). P1 first downwelled and then upwelled as it negotiated a meander trough; these cases have been separated. The change in speed, the average curvature, the equivalent radius of curvature, and the average angular distance covered by the parcel while it was tracked are also shown

Parcel	Eulerian ΔPV				Lagrangian ΔPV				Time (days)	Speed (m s ⁻¹)	κ_{av} (10 ⁻³ m ⁻¹)	Radius (km)	θ_{av}	Up/down-welling
	Δx (km)	($\times 10^3$) H (%)	Shear (%)	Stretch (%)	ΔPV (10 ⁻³) H (%)	Shear (%)	Stretch (%)	Speed (m s ⁻¹)						
P1	-18	1	+200	+100	+0.05	+200	+100	2.3	1.36±0.17	-0.47	240	0.43	0.017	Upwelling
P2	-8.5	1	+100	0	+0.10	+60	+40	2.3	1.28±0.65	-0.26	212	0.39	0.017	Upwelling
P1-1	7	-2	0	+100	-1.2	-33	-66	6.6	1.15±1.09	1.36	56	0.79	0.017	Downwelling
P1-2	-13	1.5	0	+100	+0.4	+33	+66	6.6	1.39±0.38	-0.91	109	0.92	0.017	Upwelling
P2	-4	1	+100	0	0	0	—	1.3	0.93±0.70	-0.37	278	0.29	0.017	Upwelling
P3	8	-1	-50	-50	0	0	—	1.0	0.36±1.03	0.12	833	0.06	0.017	Downwelling

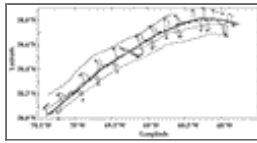
[Click on thumbnail for full-sized image.](#)

Figures



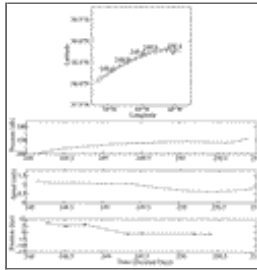
[Click on thumbnail for full-sized image.](#)

FIG. 1. Isopycnal parcels were tracked either by tagging them with acoustically tracked floats or by numerically computing their trajectories by using CTD and ADCP data. In addition to tracking the parcel, the ship also conducted CTD and ADCP surveys in the vicinity to monitor evolving density and velocity fields around the parcel. Cross-sections of PV around the parcel were constructed from these velocity and density data



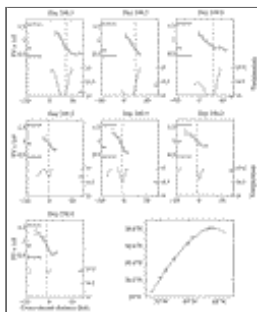
[Click on thumbnail for full-sized image.](#)

FIG. 2. Trajectory of isopycnal parcel F2 (dark solid line) and the CTD (circles with plus symbols) and ADCP (arrows show measured ADCP velocity on the isopycnal) surveys in its vicinity. The parcel crossed isobars (thin lines) on the isopycnal and upwelled when it approached the meander crest. The isobars determined from the CTD cast are spaced 60 m apart and indicate the direction of the thermal wind velocity. PV cross sections of the stream around the parcel were calculated from velocity and density sections measured nearly perpendicular to the parcel trajectory



[Click on thumbnail for full-sized image.](#)

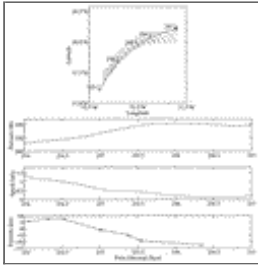
FIG. 3. (top) the trajectory of F2 as it approaches a meander crest is superposed on isobars (dashed lines with contour interval of 20 m) on $\sigma_\theta = 26.6$, showing its shoaling up the isopycnal. The numbers next to the trajectory indicate the time in days corresponding to that location. The second, third, and fourth panel show the depth, speed, and cross-stream position of the parcel (with standard error bars capturing the uncertainty in position due to uncertainty in density measurement caused by internal waves; see [section 2b](#)), which record the detrainment of the parcel from the high-speed core of the stream. For cross-stream position, origin was chosen as $\sigma_\theta = 26.5$ crossing 150 m, with positive distances offshore



[Click on thumbnail for full-sized image.](#)

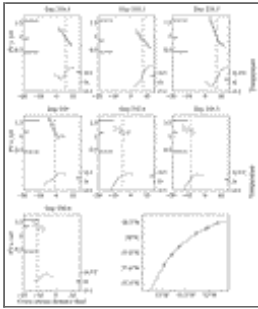
FIG. 4. Potential vorticity (with standard error bars: upper curve in each panel) and temperature (lower curve) cross sections of the stream on $\sigma_\theta = 26.6$ around F2 at various downstream locations. Time (day) corresponding to each section is shown at the top of each panel; spatial location of float at these times is shown in the last panel with plus symbols. The position of the parcel in each section is shown by the vertical line. $x = 0$ on the horizontal cross-stream axis corresponds to where $\sigma_\theta = 26.5$ crosses 150 m, with positive distances offshore. PV and temperature of the parcel at each cross section are denoted by the tick marks on the left

and right side y axes, respectively. Longer dashed tick marks on the left y axes are typical PV values for slope waters and the Sargasso Sea (see text for explanation). Onshore motion of the parcel as it approaches the crest and the onshore migration of the PV front can be seen. The $O(5 \text{ km})$ wiggles in the temperature and PV curves show the stirring of the stream and fresh cool waters, which may have originated on the shelf



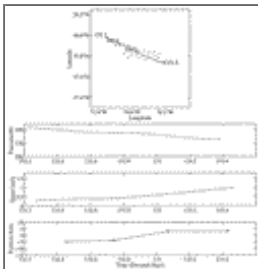
[Click on thumbnail for full-sized image.](#)

FIG. 5. As in [Fig. 3](#) but for parcel F1 detrained from the stream into the slope waters upstream of a crest, as indicated by its rapid upwelling, loss of speed, and increasingly onshore cross-stream position



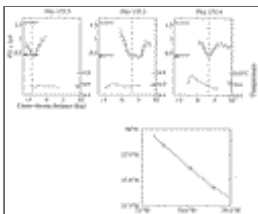
[Click on thumbnail for full-sized image.](#)

FIG. 6. Same as [Fig. 4](#) but for parcel F1 detrained from the stream into the slope waters



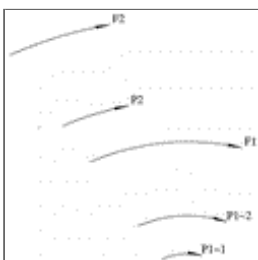
[Click on thumbnail for full-sized image.](#)

FIG. 7. As in [Fig. 3](#) but for parcel P3 entrained into the stream from the slope waters downstream of a crest, as indicated by its downwelling, increasing speed, and increasingly positive cross-stream position



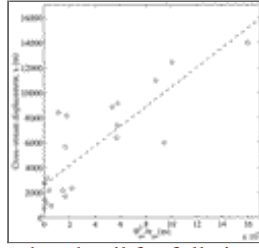
[Click on thumbnail for full-sized image.](#)

FIG. 8. As in [Fig. 4](#) but for parcel P3 entrained into the stream from the slope waters



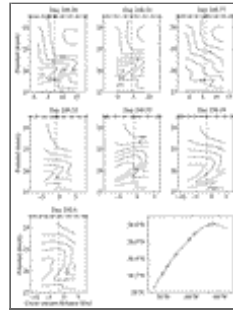
[Click on thumbnail for full-sized image.](#)

FIG. 9. Comparison of various parcel trajectories based on an average curvature (κ_{av}) and angular distance covered (θ_{av}). The radius of each arc here is proportional to the average radius of curvature for the corresponding parcel trajectory and the angle subtended by each arc is θ_{av} of the corresponding parcel in [Table 1](#). See text for details. The equivalent radius of curvature of P3 was much larger than that the others ([Table 1](#)); hence P3 was omitted from this figure. This figure allows comparison of the various parcel cases by placing them on arcs on equivalent concentric circles



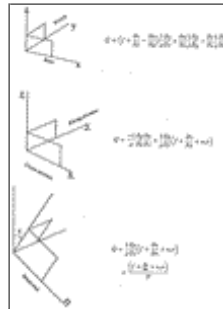
[Click on thumbnail for full-sized image.](#)

FIG. 10. The absolute value of the centrifugal force perpendicular to the parcel trajectory integrated twice with respect to time ($\theta_{av}^2/\kappa_{av}$) shows an apparent linear relationship with the absolute value of the cross-stream displacement of the parcel (x). The dashed line in the figure shows the best-fit line; the diagonal has a slope of 0.1



[Click on thumbnail for full-sized image.](#)

FIG. 11. Contours of τ , orthogonal to σ_θ in the θ - S plane, for F2 show intrusion of fresh cool waters with lower τ values into the stream. The intrusion appears weaker in successive sections taken downstream. It can be imagined that the intrusion was stretched by the velocity shear, as it flowed down the stream causing increased mixing of the fresh cool waters into the stream



[Click on thumbnail for full-sized image.](#)

FIG. A1. Ertel's PV is shown in the familiar geographical coordinate system (top); the horizontal gradients of the vertical velocity are several orders of magnitude smaller than the vertical gradients of the horizontal velocity in the Gulf Stream and have therefore been omitted. Expression for PV in a natural coordinate system (middle) where y is along the stream and x is across the stream. Expression for PV in a coordinate system (bottom) so rotated that the cross-stream axis is tangential to the isopycnals



© 2008 American Meteorological Society [Privacy Policy and Disclaimer](#)

Headquarters: 45 Beacon Street Boston, MA 02108-3693

DC Office: 1120 G Street, NW, Suite 800 Washington DC, 20005-3826

amsinfo@ametsoc.org Phone: 617-227-2425 Fax: 617-742-8718

[Allen Press, Inc.](#) assists in the online publication of *AMS* journals.